2021 IEEE 22nd International Workshop on Signal Processing Advances in Wireless Communications (SPAWC) | 978-1-6654-2851-4/21/$31.00 ©2021 IEEE | DOI: 10.1109/SPAWC51858.2021.9593249

Fundamentals of Circular QAM for Wireless Information and Power Transfer

Ghassan M. Kraidy*†, Constantinos Psomas*, and Ioannis Krikidis*
*Department of Electrical and Computer Engineering, University of Cyprus, Cyprus
†Department of Electrical, Computer and Communication Engineering, Notre Dame University - Louaize, Lebanon
Email: {kraidy.ghassan, psomas, krikidis}@ucy.ac.cy

***Abstract*—In this work, circular quadrature amplitude modulation (CQAM) is investigated for simultaneous wireless information and power transfer (SWIPT). Both coded and uncoded cases are considered, under which the flexibility of CQAM for SWIPT is presented. Specifically, for uncoded transmission, CQAM is designed to achieve a controllable tradeoff between energy harvesting and information transfer performance. In the coded case, bit-interleaved coded-CQAM are designed based on the maximization of the discrete-input capacity. Our results show, in both cases, the superiority of CQAM compared to known modulation schemes (*i.e.* QAM, PSK, and PAM) in terms of error rate and energy harvesting.**

***Index Terms*—Wireless power transfer, energy harvesting, SWIPT, coded modulation, CQAM.**

I. Introduction

SIMULTANEOUS wireless information and power transfer (SWIPT) is a new wireless technology, where information and energy are co-designed into the same radio-frequency signal to communicate and energize [1]. It is a promising solution for future wireless networks, which are characterized by a massive number of low-rate low-power devices such as in the Internet of Things. Due to the nonlinearity of the rectification circuit, SWIPT efficiency highly depends on the shape of the transmitted signal and requires radical re-design of the input distribution, modulation, waveform, beamforming, and a combination thereof [2].

The investigation of modulation techniques for SWIPT has been scarcely addressed in the literature. By exploiting the fundamental observation that signals with high peak-to-average power ratio (PAPR) are more appropriate for transferring energy [2], [3], the authors in [4] compare conventional communication modulations (*i.e.* PAM, PSK, QAM) in terms of SWIPT. More recent works investigate beyond state-of-the-art modulation schemes by taking into account the nonlinearity of the rectification process. The authors in [5], design an asymmetric PSK, where symbols are distributed in a limited phase range and achieve higher rate-energy tradeoff regimes. On the other hand, the authors in [6] study optimal modulation constellations when both transmitter and receiver are implemented using deep neural network-based autoencoders, while the authors in [7] propose a SWIPT-based modulation scheme based on probabilistic shaping. Furthermore, in [8] and [9], the authors propose circular constellations to approach a rate-energy region. The aforementioned works do not consider the tradeoff between the minimum Euclidean distance and the PAPR. Indeed, they provide fixed constellations with high energy symbols and a cloud of symbols centered at the origin that penalizes the error rate performance. However, one can boost energy harvesting by increasing PAPR at the expense of the information transfer performance.

This work has received funding from the European Research Council (ERC) under the European Union's Horizon 2020 research and innovation programme (Grant agreement No. 819819).

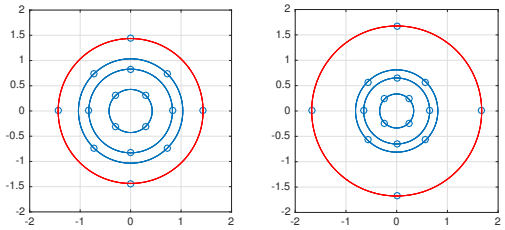

Fig. 1. CQAM modulation with $M = 16$, $N = 4$, a) designed for best performance (*i.e.* highest $d_{\min}$), and b) designed for better energy harvesting performance (*i.e.* higher PAPR).

In this work, we propose the design of circular quadrature amplitude modulation (CQAM) [10] for SWIPT. Specifically, by placing modulated symbols on different levels (*i.e.* on different circles within the signal space diagram), CQAM allows to tune the amount of energy to be harvested without affecting the performance. As CQAM consists of a simple re-positioning of symbols within the two-dimensional signal space diagram, they can be implemented with the same hardware used for classical modulation schemes. The design of CQAM for SWIPT is first proposed for uncoded transmissions, which provides a controllable tradeoff between energy harvesting and information transfer. Then, we consider the case of coded-CQAM based on discrete-input capacity maximization. Our results on symbol error rate (SER) and word error rate (WER) show the superiority of CQAM compared to other conventional modulation schemes.

II. System Model

Consider a single-input single-output point-to-point SWIPT system, where the receiver can jointly harvest energy and decode information. We assume that the transmitter adopts the CQAM modulation scheme, in which the modulated symbols are distributed over N circles (or energy levels) with radii $R_1 < R_2 < \cdots < R_N$ [10]. As an example, the constellation

in Fig. 1(a) has size $M = 16$ symbols with $N = 4$ circles, meaning there are $n = M/N = 4$ symbols per circle. Note that, unlike in [10], the CQAM considered in this paper is not restricted to the case where $n = N$. In a goal to study the fundamental characteristics of CQAM for SWIPT, we consider transmission over an additive white Gaussian noise (AWGN) channel, as was investigated in [11], [12]. This channel serves as a useful guideline for later considerations of more realistic channels, such as fading for instance. Thus, the baseband channel model is given by

$$y = hx + \eta, \tag{1}$$

where x is a $M = 2^m$ complex baseband modulated symbol with m bits per symbol, y is the baseband received signal, and η is an AWGN realization with zero mean and variance $2N_0$. The fading coefficient h is constant and known at the transmitter and the receiver (for simplicity, we set $h = 1$ [11]).

For energy transfer, a nonlinear rectification circuit that converts the received radio-frequency (RF) signal to direct current (DC) power is considered. The receiver employs the *power splitting* technique and so a fraction ρ of the received signal's power is used to harvest energy, while the remaining $(1 - \rho)$ is used for information transfer [4]. Therefore, the amount of harvested energy is given by[1]

$$\varepsilon(x) = \alpha T_s \left(\rho P_r - P_{th}\right)^+, \tag{2}$$

where T_s is the symbol duration, $0 \leq \alpha \leq 1$ is the RF-DC efficiency, $P_r = E[|x|^2]$ is the received symbol power (where $E[\cdot]$ denotes expectation), P_{th} is the power threshold above which energy is harvested, and $a^+ = \max\{0, a\}$. As modulations with higher PAPR increase the DC output of the rectifier [3], in what follows, we focus on the tradeoff between PAPR and the minimum Euclidean distance of CQAM. Specifically, with CQAM, the amplitude levels of the modulated symbols are given by the radius of the circle to which they belong. The PAPR can thus be written as

$$\text{PAPR} = \frac{R_N^2}{E_i[R_i^2]}. \tag{3}$$

Now, as the energy harvesting performance is a function of the PAPR, the next section will focus on the design of CQAM whose PAPR is increased given the minimum distance of the constellation.

III. CQAM DESIGN FOR SWIPT

A. Uncoded transmission

According to the literature [2], [3], it has been shown that the best modulation schemes in terms of energy harvesting are the ones that have the highest PAPR. However, these modulation schemes face error rate performance degradation, as their minimum Euclidean distance decreases. For this reason, the CQAM family proposed in this letter allows for the design of a flexible tradeoff between PAPR and $d_{\min}$. Moreover, the number of levels N has a direct effect on the PAPR, as the larger the N, the higher the values the PAPR can reach. A thorough analysis on the impact of the parameters of CQAM on PAPR is given in Appendix A.

Algorithm 1: CQAM design for maximum PAPR

Input: $d_{\min}$, M, N
Output: $\mathbf{s}_1, \ldots, \mathbf{s}_N$
$n \leftarrow M/N$
$R_1 \leftarrow \frac{d_{\min}}{2\sin(\pi/n)}$
for $i \leftarrow 1$ *to* $N-1$ **do**
  $\mathbf{s}_i \leftarrow n$ symbols at level R_i such that $\text{dist}(\mathrm{s}_{ij}, \mathrm{s}_{ik}) \geq d_{\min}$ and $\text{dist}(\mathrm{s}_{ij}, \mathrm{s}_{wk}) \geq d_{\min}$
end
Find $\mathbf{s}_N$ such that $\text{dist}(\mathrm{s}_{Nj}, \mathrm{s}_{(N-1)k}) \geq d_{\min}$ and $E_i[R_i^2] = 1$
Return $\mathbf{s}_1, \ldots, \mathbf{s}_N$

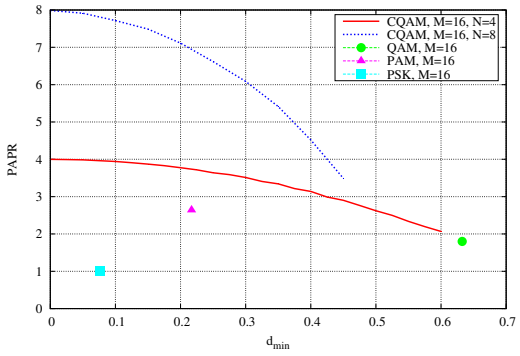

Fig. 2. PAPR versus $d_{\min}$ of CQAM and some well-known modulation schemes.

The construction of CQAM is based on the method from [10] that is hereby summarized: first, the inner circle with radius R_1 is considered. If we suppose there are n constellation points per circle that are separated by an angle of $2\pi/n$, the distance between points located in the inner circle is $d_1 = 2R_1 \sin(\pi/n)$[2]. As R_1 is the smallest radius, this distance will represent the minimum Euclidean distance of CQAM, i.e. $d_{\min} = d_1$. The next step would be to find R_2; as $R_2 > R_1$, we have that $d_2 = 2R_2 \sin(\pi/n) > d_{\min}$, which means R_2 is chosen that the distance between any symbol on R_1 and any symbol on R_2 should be at least $d_{\min}$. The same procedure is applied to the remaining consecutive circles up to the outermost circle with radius R_N. Now as the goal is to achieve a higher PAPR, CQAM design would be slightly modified; first, R_1 is decreased, since this will also decrease $d_{\min}$. The constellation points on circles with radii up to R_{N-1} are then found such that points are distanced at $d_{\min}$. This means that, for the same average energy, R_N will take a larger value and thus increase the PAPR (see (3)). The design steps are summarized in Algorithm 1. It is worth mentioning that,

[1]This is a piecewise linear model that captures the energy harvesting sensitivity and that is sufficient for the purpose of our work. Other nonlinear models can be also considered without loss of generality.

[2]The Euclidean distance d between two points on a circle of radius r separated by an angle θ is $d = 2r\sin(\pi/(2\theta))$.

as $R_1 = d_{\min}/(2\sin(\pi/n))$, the PAPR in (3) can be obtained as a function of $d_{\min}$.

Fig. 2 shows the PAPR behavior versus $d_{\min}$ of 16-CQAM with 4 and 8 levels compared with known modulation schemes, namely 16-PAM, 16-PSK, and 16-QAM. For CQAM, the value of the radii was changed so that, for a given minimum allowable $d_{\min}$, the constellation with the highest PAPR was found. Hence, each point on the curves of Fig. 2 represents a constellation having a specific PAPR for a given $d_{\min}$. Note that, for $d_{\min} = 0$, we have $R_1 = R_2 = \cdots = R_{N-1} = 0$ and $R_N = N$, which results in PAPR = N. All the modulation schemes in this figure have unit average energy. With CQAM, it is clear that the design tradeoff allows for trading PAPR for $d_{\min}$, outperforming 16-PAM in terms of PAPR, while getting very close to the performance level of 16-QAM. Moreover, it can be seen that a CQAM with more levels allows to achieve higher PAPR values, however the error rate performance becomes poorer. By allowing to modify the number of energy levels and by allowing to trade PAPR with minimum Euclidean distance, CQAM introduces a flexibility in the design that is not possible in known modulation schemes.

In terms of SER under maximum likelihood (ML) detection, the performance of CQAM with energy harvesting is approximated by the nearest neighbor approximation [15] as

$$P_e \approx \frac{1}{N}\sum_{i=1}^{N} \nu(i) Q\left[\sqrt{\frac{E_b}{N_0}\sin(\pi/n)\left(\sqrt{R_i^2 - \varepsilon(R_i)}\right)^+}\right], \tag{4}$$

where

$$\varepsilon(R_i) = \left(\rho R_i^2 - \alpha T_s P_{th}\right)^+, \tag{5}$$

is the energy harvested at level R_i based on (2), $\nu(i)$ represents the number of neighbors at the minimum distance at level i, and $Q[\cdot]$ is the Q-function. After harvesting, the energy remaining for information transfer is $R_i^2 - \varepsilon(R_i)$, resulting in the signal space diagram of the constellation to shrink towards the origin. This means that the minimum distance between symbols at level i is given by

$$d_{\min}(i) = 2\sin(\pi/n)\left(\sqrt{R_i^2 - \varepsilon(R_i)}\right)^+, \tag{6}$$

which reduces to $d_{\min}(i) = 0$ when all the energy at level i is used for harvesting (*i.e.* when $\varepsilon(R_i) = R_i^2$). In this case, the error rate at level i is $Q[0] = 0.5$, as there is no observation on the symbol at the output of the channel. When most symbols are used exclusively for harvesting, the error rate curve suffers from a high error floor, as reliable demodulation becomes impossible at the receiver; this is shown in Section IV.

B. Coded transmission

In the coded case, digital transmission is performed as follows: an information packet of length K bits is fed to a recursive systematic convolutional (RSC) code that generates P parity bits. The coding rate is thus $R_c = K/(K+P)$. The resulting codeword C of length $\ell = K + P$ bits is then fed to an interleaver before being modulated and sent over the channel. The modified baseband channel model is given by

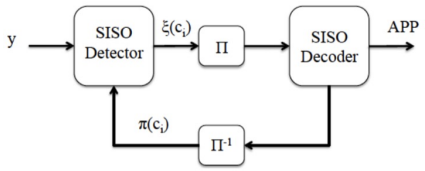

Fig. 3. Iterative *a posteriori* probability detection and decoding receiver.

$$y_k = x_k + \eta_k, \quad k = 1, \cdots, \ell/m. \tag{7}$$

The receiver consists of a soft detector that generates extrinsic probabilities $\xi(c_i)$ on received bits $c_i \in C$ based on symbol y_k and *a priori* probabilities $\pi(c_u)$ as

$$\begin{aligned}\xi(c_i) &= \frac{p(y_k|c_i=1)}{p(y_k|c_i=0)+p(y_k|c_i=1)} \\ &= \frac{\sum_{x'\in\mathcal{X}(c_i=1)}\left[\exp\left(-||y_k - x'_k||^2/2N_0\right)\prod_{u\neq i}\pi(c_u)\right]}{\sum_{x\in\mathcal{X}}\left[\exp\left(-||y_k - x_k||^2/2N_0\right)\prod_{u\neq i}\pi(c_u)\right]},\end{aligned} \tag{8}$$

where $\mathcal{X}$ represents the CQAM constellation. The extrinsic probabilities are then deinterleaved before being fed to a soft-input soft-output "Forward-Backward" decoder [13] that generates extrinsic probabilities on the bits. The extrinsic probabilities are then fed to an interleaver and back to the detector. After a few iterations, a decision on the information bits is made at the output of the decoder based on their *a posteriori* probabilities, as shown in Fig. 3.

It is well known that capacity is achieved over AWGN channels with a Gaussian distribution at the input of the channel. However, when transmitting modulated symbols, the input to the channel becomes discrete, as one out of M possible symbols is transmitted at a time. In this case, the capacity with discrete input (*i.e.* modulation $\mathcal{X}$) is given by [14]

$$C(\mathcal{X}) = \log_2(M) - E\left[\log_2\left(\frac{\sum_{x'} p\left(y|x'\right)}{p\left(y|x\right)}\right)\right], \tag{9}$$

where expectation is over the noise variable and

$$p\left(y|x\right) \propto \exp\left(-\frac{||y-x||^2}{2N_0}\right). \tag{10}$$

As $C(\mathcal{X})$ for a given modulation scheme is upper-bounded by the Gaussian-input capacity, the design of CQAM for coded transmission consists of finding the CQAM constellation $\mathcal{X}^*$ that maximizes the discrete-input capacity as

$$\mathcal{X}^* = \arg \max_{x\in\aleph} C(\mathcal{X}), \tag{11}$$

where $\aleph$ represents the ensemble of CQAM modulations with a given number of symbols M and number of levels N. The expression for the capacity in (9) can be simplified as

$$\begin{aligned}C(\mathcal{X}) &= m - \frac{1}{M}\sum_{i=1}^{M-1} E\left[\log_2\sum_{i=1}^{M-1}\exp\left(-\frac{|x_i+\eta-x_j|^2-|\eta|^2}{2N_0}\right)\right] \\ &= m - \frac{1}{M}\sum_{i=1}^{M-1} E\left[\log_2\sum_{i=1}^{M-1}\exp\left(-\frac{|x_i-x_j|^2-2|\eta||x_i-x_j|}{2N_0}\right)\right].\end{aligned} \tag{12}$$

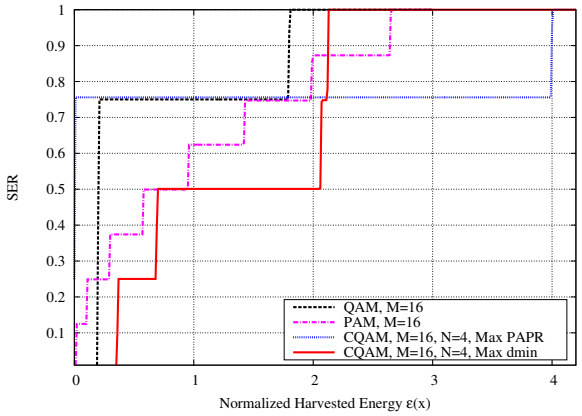

Fig. 4. SER versus normalized harvested energy $\varepsilon(x)$ of several modulation schemes with $M = 16$ symbols.

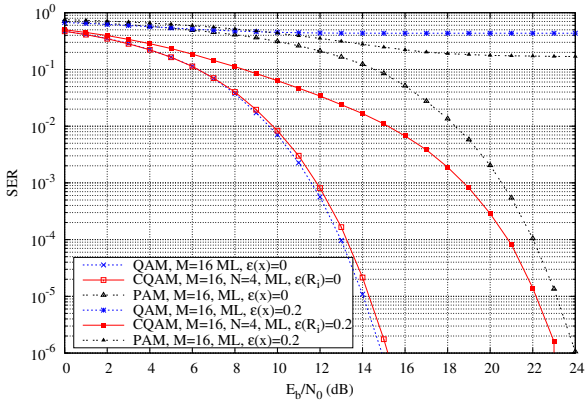

Fig. 5. SER of various uncoded modulation schemes under maximum likelihood detection.

Now, if we consider all the pairs $|x_i - x_j|$, the smallest difference corresponds to terms that are at the minimum Euclidean distance $d_{\min}$ from each others, meaning that, for high signal-to-noise ratio (SNR) (*i.e.* for small N_0), we have

$$\sum_{i=1}^{M-1} \exp\left(-\frac{|x_i - x_j|^2 - 2|\eta||x_i - x_j|}{2N_0}\right) \approx \exp\left(-\frac{d_{\min}^2 - 2|\eta|d_{\min}}{2N_0}\right). \quad (13)$$

Therefore, an approximation of $C(\mathcal{X})$ is now given by

$$\begin{aligned} C(\mathcal{X}) &\approx m - \frac{1}{M}\sum_{i=1}^{M-1} E\left[\log_2 \exp\left(-\frac{d_{\min}^2 - 2|\eta|d_{\min}}{2N_0}\right)\right] \\ &\approx m - \frac{1}{M}\sum_{i=1}^{M-1} E\left[\frac{-d_{\min}^2 + 2|\eta|d_{\min} + 2N_0}{\log(2)}\right] \\ &\approx m + \frac{d_{\min}^2 - 2N_0}{\log(2)}. \end{aligned} \quad (14)$$

The above expression shows that for a given constellation size with m bits per symbol and noise variance $2N_0$, the discrete-input capacity over AWGN channels is a function of the minimum Euclidean distance $d_{\min}$. As such, the same observations as with the uncoded case apply here as well. In particular, coded CQAM can achieve a certain SER performance with higher $\varepsilon(R_i)$ compared to other schemes, thus harvesting more energy.

IV. Simulation Results

In this section, error rate curves versus the SNR of CQAM with SWIPT are shown under Monte Carlo simulations. Fig. 4 shows the SER versus $\varepsilon(x)$ from (2) of several modulation schemes with unit average energy. We set $P_{th} = 0$ which gives: $\sqrt{R_i^2 - \varepsilon(R_i)} = R_i\sqrt{(1-\rho)}$ in (4) which corresponds to the *power splitting* expression from [4]. The channel is an AWGN at very high SNR. For existing modulation schemes, 16-QAM represents the best performing scheme, while 16-PAM has the highest PAPR, giving the best energy harvesting performance. These schemes are compared with 16-CQAM with $N = 4$ levels, and it is clear that CQAM can be designed to perform better in terms of SER (red curve) or energy harvesting (blue curve) than existing modulation schemes.

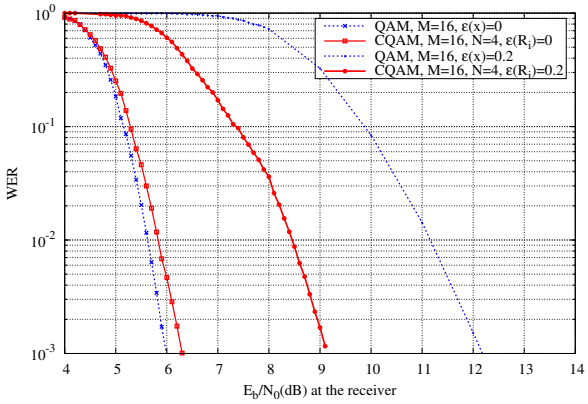

Fig. 6. WER of coded modulations, $R_c = 1/2$ NRNSC $(133, 171)_8$ code, interleaver size $\ell = 1000$ bits, s-random interleaving, iterative receiver.

In Fig. 5, SER results of 16-CQAM with $N = 4$ energy levels are shown with 16-QAM and 16-PAM. In the absence of energy harvesting at the receiver (*i.e.* $\varepsilon(R_i) = 0$ and $\varepsilon(x) = 0$ for other modulation types), CQAM performance is almost as good as the best 16-level modulation scheme, namely QAM. However, as soon as a fraction of energy of 0.2 is used for energy harvesting, CQAM clearly outperforms all existing schemes that suffer from an error floor (including 16-PAM which is known for its energy harvesting performance [4]).

In Fig. 6, WER performance of coded-CQAM is shown. The error correcting code used is the non-recursive non-systematic convolutional (NRNSC) half-rate code with generator polynomials $(133, 171)_8$ that is used in the IEEE802.11 standard. The binary mapping used consists of maximizing the harmonic mean of the Euclidean distance of constellation points [16], as this ensures a better iterative receiver performance than Gray mapping. The interleaver separating the code from the modulator is an S-random interleaver [17] with $s = 12$, and the codeword (or interleaver) length is $\ell = 1000$ bits. Again, 16-CQAM with $N = 4$ levels is compared to 16-QAM, with

similar observations as with uncoded transmission: almost similar performance in the absence of energy harvesting, while CQAM outperforms QAM by almost 3 dB whenever $\varepsilon(x) = \varepsilon(R_i) = 0.2$.

V. Conclusion

In this letter, the design of CQAM for SWIPT has been proposed, that allows for an efficient tradeoff between the harvested energy and the energy used for information transfer. Both uncoded transmission and coded modulation have been investigated, and it was shown that the tradeoff between the PAPR and the minimum Euclidean distance of the constellation determines the SWIPT performance in both cases. Finally, simulated error rate curves have highlighted the superiority of CQAM with respect to known modulation schemes. In the future, the design of CQAM with probabilistic constellation shaping will be investigated, as well as the performance of CQAM for SWIPT in the presence of channel fading.

Appendix A
Analysis of PAPR with CQAM

The impact of the CQAM parameters on the PAPR is hereby investigated. Let N be the number of levels and let Δ be the spacing between any two consecutive levels. Then, the PAPR can be written as

$$\begin{aligned}\text{PAPR} &= \frac{N\left(R_1+(N-1)\Delta\right)^2}{\frac{1}{N}\sum_{i=1}^{N}\left(R_1+(i-1)\Delta\right)^2} \\ &= \frac{1}{N}\sum_{i=1}^{N}\left(E_i[R_i]-R_1-(i-1)\Delta\right)^2. \end{aligned} \quad (15)$$

By setting $N = 4$, we obtain

$$\text{PAPR} = \frac{R_1^2+6\Delta R_1+9\Delta^2}{R_1^2+3\Delta R_1+3.5\Delta^2}, \quad (16)$$

and for $N = 8$, we obtain

$$\text{PAPR} = \frac{R_1^2+14\Delta R_1+49\Delta^2}{R_1^2+7\Delta R_1+17.5\Delta^2}. \quad (17)$$

Now, if $R_1 = 1$, (16) becomes

$$\text{PAPR} = \frac{18\Delta+12}{7\Delta+6}, \quad (18)$$

and (17) becomes

$$\text{PAPR} = \frac{14\Delta+4}{5\Delta+2}. \quad (19)$$

It is clear from (18) and (19) that the PAPR increases with the number of levels.

Next, we provide asymptotic expressions for the PAPR so as to show the behavior for large N and large values of Δ. First, the mean-square value of the radii is given by

$$\begin{aligned}E_i[R_i^2] &= \frac{1}{N}\sum_{i=1}^{N}\left[\left(R_1+(i-1)\Delta\right]^2\right. \\ &= R_1^2+\frac{\Delta^2}{N}\sum_{i=1}^{N-1}i^2+\frac{2\Delta R_1}{N}\sum_{i=1}^{N-1}i \\ &= R_1^2+\frac{\Delta^2}{6}(N-1)(2N-1)+\Delta R_1(N-1). \end{aligned} \quad (20)$$

Using (20), PAPR can be evaluated as

$$\text{PAPR} = \frac{R_1^2+\Delta^2(N-1)^2+2\Delta R_1(N-1)}{R_1^2+\frac{\Delta^2}{6}(N-1)(2N-1)+\Delta R_1(N-1)}. \quad (21)$$

Then, by considering the asymptotic cases $\Delta \to \infty$ and $N \to \infty$, (21) converges to

$$\lim_{\Delta\to\infty}\text{PAPR} = \frac{6(N-1)}{2N-1}, \quad (22)$$

and

$$\lim_{N\to\infty}\text{PAPR} = 3, \quad (23)$$

respectively. Therefore, as Δ becomes large, the PAPR becomes independent of the radii R_i and depends only on N. Moreover, for equally spaced energy levels, the PAPR converges to a constant as N goes to infinity, regardless of the values of N and R_i. However, there is no need to impose equal spacing, as constellation points on outer circles have inherent large distances between them, meaning that Δ can be allowed to decrease.

References

[1] B. Clerckx, R. Zhang, R. Schober, D. W. K. Ng, D. I. Kim, and H. V. Poor, "Fundamentals of wireless information and power transfer: From RF energy harvester models to signal and system designs," *IEEE J. Selec. Areas Comm.*, vol. 37, pp. 4–33, Jan. 2019.

[2] B. Clerckx and E. Bayguzina, "Waveform design for wireless power transfer," *IEEE Trans. Signal Proc.*, vol. 64, pp. 6313–6328, Dec. 2016.

[3] D. I. Kim, J. H. Moon, and J. J. Park, "New SWIPT using PAPR: How it works," *IEEE Wireless Comm. Lett.*, vol. 5, pp. 672–675, Dec. 2016.

[4] W. Liu, X. Zhou, S. Durrani, and P. Popovski, "SWIPT with practical modulation and RF energy harvesting sensitivity," *Proc. IEEE Int. Conf. Comm.*, Kuala Lumpur, Malaysia, May 2016, pp. 1–7.

[5] E. Bayguzina and B. Clerckx, "Asymetric modulation design for wireless information and power transfer with nonlinear energy harvesting," *IEEE Trans. Wireless Comm.*, vol. 18, pp. 5529–5541, Dec. 2019.

[6] M. Varasteh, E. Piovano, and B. Clerckx, "A learning approach to wireless information and power transfer signal and system design," *Proc. IEEE Int. Conf. Acoust. Speech Sign. Proc.*, Brighton, UK, May 2019.

[7] A. Rajaram, D. N. Jayakody, B, Chen, R. Dinis, and S. Affes, "Modulation-based simultaneous wireless information and power transfer," *IEEE Comm. Lett.*, vol. 24, pp. 136–140, Jan. 2020.

[8] C. Thomas, M. Weidner, and S. Durrani, "Digital amplitude-phase keying with M-ary alphabets," *IEEE Trans. Comm.*, vol. 22, pp. 168–180, Feb. 1974.

[9] Y.-B. Kim, D. K. Shin, and W. Choi, "Rate-energy region in wireless information and power transfer: New receiver architecture and practical modulation," *IEEE Trans. Comm.*, vol. 66, pp. 2751–2761, June 2018.

[10] J. Van Wonterghem, J. J. Boutros, and M. Moeneclaey, "Construction of Circular Quadrature Amplitude Modulations (CQAM)," *IEEE Int. Conf. on the Science of Elec. Eng.. (ICSEE'18)*.

[11] R. Morsi, V. Jamali, D. W. K. Ng, and R. Schober, "On the capacity of SWIPT systems with a nonlinear energy harvesting circuit" *Proc. IEEE Int. Conf. Comm.*, Kansas City, USA, May 2018, pp. 1–7.

[12] L. R. Varshney, "Transporting information and energy simultaneously," in *Proc. IEEE Int. Symp. Inf. Theory*, Toronto, Canada, July 2008.

[13] F. Jelinek J. Raviv L. Bahl, and J. Cocke, "Optimal decoding of linear codes for minimizing symbol error rate," *IEEE Trans. Inf. Theory*, vol. 20, pp. 284–287, Mar. 1974.

[14] G. Ungerboeck, "Channel coding with multilevel/phase signals," *IEEE Trans. Inf. Th.*, vol. 28, pp. 55–67, Jan. 1982.

[15] A. Goldsmith, "Wireless communications," *Cambridge Univ. Pr.*, 2008.

[16] A. Chindapol and J.A. Ritcey, "Design, analysis, and performance evaluation for BICM-ID with square QAM constellations in Rayleigh fading channels," *IEEE J. Sel. Areas Comm.*, vol. 19, pp. 944–957, May 2001.

[17] S. Crozier and P. Guinand, "High-performance low-memory interleaver banks for turbo-codes," in *Proc. IEEE Vehic. Tech. Conf. Fall*, Atlantic City, NJ, USA, 2001.